

Quantum-mechanical simulation of MgAl_2O_4 under high pressure

L. Gracia,¹ A. Beltrán,¹ J. Andrés,¹ R. Franco,² and J. M. Recio^{1,2}

¹*Departament de Ciències Experimentals, Universitat Jaume I, E-12080 Castelló, Spain*

²*Departamento de Química Física y Analítica, Universidad de Oviedo, E-33006 Oviedo, Spain*

(Received 26 July 2002; published 31 December 2002)

The equations of state and phase diagrams of the cubic spinel and two high-pressure polymorphs of MgAl_2O_4 have been investigated up to 65 GPa using density functional theory, the space-filling polyhedral partition of the unit cell, and the static approximation. Energy-volume curves have been obtained for the spinel phase, the recently observed calcium ferrite-type and calcium titanite-type phases, and the $\text{MgO} + \alpha\text{-Al}_2\text{O}_3$ mixture. Zero-pressure unit lengths and compressibilities are well described by the theoretical model, that predicts static bulk moduli about 215 GPa for all the high-pressure forms. Computed equations of state are also in good agreement with the most recent experimental data for all compounds and polymorphs considered. We do not find a continuous pressure-induced phase sequence but the static simulations predict that the oxide mixture, the ferrite phase, and the titanite phase become more stable than the spinel form at 15, 35, and 62 GPa, respectively. A microscopic analysis in terms of polyhedral and bond compressibilities leads to identify the ionic displacements accompanying the phase transformations and to an appealing interpretation of the spinel response to compression.

DOI: 10.1103/PhysRevB.66.224114

PACS number(s): 64.60.-i, 71.15.Nc, 61.50.Ks, 61.50.Lt

I. INTRODUCTION

In the last decades there has been an increasing interest in understanding the high-pressure behavior of MgAl_2O_4 . This technologically important compound crystallizes in the cubic spinel structure at normal conditions. Besides its electronic applications and prototypical character for ceramics, MgAl_2O_4 plays a significant role in geophysics¹ as one of the early condensed minerals and a common constituent of the shallow upper mantle. The elastic behavior of its polymorphs can be used to predict seismic velocities, and some of its high-pressure forms have been proposed as constituents of shock-metamorphosed meteorites.

Although as early as 1969 Reid and Ringwood suggested two orthorhombic structures, the calcium ferrite-type phase (F phase from now on) and the calcium titanite-type phase (T phase from now on), as high-pressure forms for MgAl_2O_4 ,² their structure and equation of state (EOS) have not been fully characterized until very recently.^{1,3,4} The observed unit lengths of the quenched F phase at zero pressure are consistent, but the zero-pressure bulk modulus (B_0) varies from 211 GPa (Ref. 4) to 241 GPa (Ref. 3). Earlier static compression measurements⁵ revealed that the cubic spinel phase (S phase from now on) decomposes into its simple oxides ($\text{MgO} + \alpha\text{-Al}_2\text{O}_3$) at 15 GPa and 1000 °C. Further pressure loading (~ 25 GPa) in shock-wave experiments led to the proposal of a phase some 20% denser than spinel and labeled $\epsilon\text{-MgAl}_2\text{O}_4$.⁶ More recent shock recovery experiments⁷ could not confirm the existence of this phase. Moreover, no evidence of it was detected in the experiments of Irifune *et al.*,¹ and only traces were suggested by Funamori *et al.*⁴ In addition, the room-temperature compression measurements of Kruger *et al.*⁸ indicated that the S structure remains as (meta)stable from 0 to 65 GPa. In the latter work, an accurate S EOS is given by fitting B_0 and its pressure derivatives B'_0 and B''_0 to all the p - V data available.

Calculations on the pressure effects on MgAl_2O_4 were mainly directed to the S phase and its decomposition into $\alpha\text{-Al}_2\text{O}_3$ and MgO .⁹⁻¹³ Catti *et al.* studied the solid state $\text{MgO} + \alpha\text{-Al}_2\text{O}_3 \rightarrow \text{MgAl}_2\text{O}_4$ reaction to determine the equilibrium diagram of these systems.¹⁰ They predicted a zero-temperature decomposition pressure of 11 GPa, in agreement with the experimental data, and gave Mg-O and Al-O bond compressibilities up to 25 GPa. They also computed the elastic behavior of the two phases and found a B_0 value for spinel some 10% larger than the observed. More recently,^{12,13} a microscopic analysis was proposed to understand the compressibility of the S phase in terms of ionic or polyhedral contributions. These studies could explain the known common response of the oxide spinels to applied pressure and prompted us to extend the theoretical analysis to the orthorhombic structures recently discovered. As far as we know, only the T phase has been theoretically studied.¹⁴ This very recent density-functional-theory (DFT) work includes local density approximation (LDA) and nonlocal (B3LYP) analyses, and describes well the unit cell geometry and the phase stability diagram, but gives $B_0(\text{LDA}) = 248$ GPa and $B_0(\text{B3LYP}) = 222$ GPa.

The aim of this work is to investigate the pressure-induced polymorphism of MgAl_2O_4 from a microscopic point of view. Preliminary results were presented elsewhere.¹⁵ We used the CRYSTAL98 (Ref. 16) code to perform DFT calculations of the crystal total energy as a function of the unit-cell volume. From these calculations we determined the equilibrium geometry for any given pressure in the $0 \leq p \leq 65$ GPa range. Then we invoked the partition of the unit cell into space-filling elementary polyhedra to write down the bulk compressibility as a weighted sum of polyhedral compressibilities¹⁷ and to give a microscopic interpretation of the pressure response of this crystal in terms of ionic displacements. This approach gives a plausible quantitative description of the behavior of MgAl_2O_4 up to 65 GPa, and an interesting correlation between the computed phases dia-

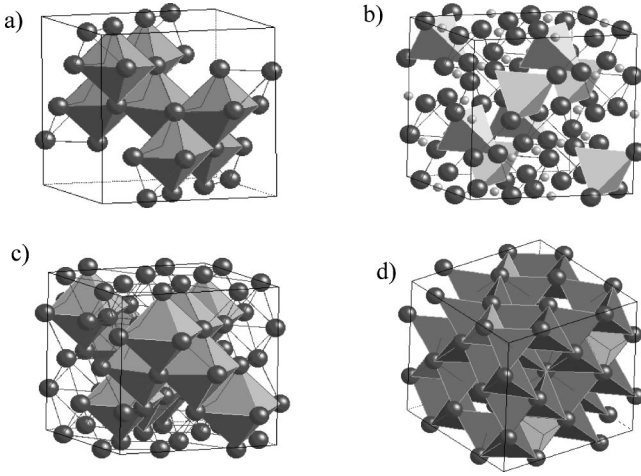


FIG. 1. Polyhedral arrays in the cubic spinel structure of MgAl_2O_4 : (a) AlO_6 , (b) MgO_4 , (c) O_6 , and (d) $(\text{O}_4)_1$ and $(\text{O}_4)_2$.

gram and the crystal structure.

Section II contains the algebra of the polyhedral partition and the computational details of the total energy calculation. In Sec. III we present a microscopic analysis of the spinel compressibility, the calculated structure, and the EOS of the two orthorhombic phases, and a discussion of the isothermal phase diagram. Our conclusions are collected in Sec. IV.

II. COMPUTATIONAL MODELING

A. Polyhedral partition of the spinel unit cell

The cubic spinel belongs to the $Fd\bar{3}m$ group, and its unit cell contains eight MgAl_2O_4 molecules. The oxide ions at the (u, u, u) positions form a distorted faced-centered-cubic packing. The eight Mg^{2+} ions at $(\frac{1}{8}, \frac{1}{8}, \frac{1}{8})$ occupy the center of tetrahedral interstices and the 16 Al^{3+} ions at $(\frac{1}{2}, \frac{1}{2}, \frac{1}{2})$ are the centers of the octahedral interstices. Since this unit cell has 64 tetrahedral and 32 octahedral holes, there are 56 empty tetrahedra and 16 empty octahedra. The smaller size and larger charge of the Al^{3+} cation produces a u value larger than 1/4, the ideal or regular close-packing value. For the same reason, the occupied tetrahedral (octahedral) interstices are larger (smaller) than the ideal ones.

The unit cell can be partitioned into five types of polyhedra that fill completely its volume: AlO_6 , MgO_4 , O_6 , $(\text{O}_4)_1$, and $(\text{O}_4)_2$, with multiplicities $n_p = 16, 8, 16, 8$, and 48, respectively (see Fig. 1). Thus, analytical expressions relating the crystal compressibility κ to the polyhedral compressibilities κ_p can be derived.^{12,17} We will use the subscripts ‘‘oct’’ and ‘‘tet’’ for the octahedral and tetrahedral case, respectively. Superscript ‘‘ ϕ ’’ will designate an empty polyhedron.

The polyhedral volumes V_p can be expressed in terms of the cell volume V_{cell} or the molecular volume V as simple algebraic functions of the internal parameter u ,¹⁸

$$V_{\text{oct}} = 128V \cdot u \cdot u_{38}^2/3, \quad V_{\text{tet}} = 64V \cdot |u_{18}|^3/3,$$

$$V_{\text{oct}}^\phi = 128V \cdot u_{18}^2 \cdot |u_{12}|/3,$$

$$V_{\text{tet1}}^\phi = 64V \cdot |u_{38}|^3/3, \quad V_{\text{tet2}}^\phi = 8V \cdot |u_{18}| \cdot |u_{38}|/3, \quad (1)$$

where $u_{ij} = u - i/j$.

The isothermal polyhedral compressibilities are the inverse of the polyhedral compressibility moduli B_p ,

$$\kappa_p = \frac{1}{B_p} = -\frac{1}{V_p} \left(\frac{\partial V_p}{\partial p} \right), \quad (2)$$

and they can be written in the general form

$$\kappa_p = \kappa - g_p \left(\frac{\partial u}{\partial p} \right), \quad (3)$$

where

$$g_{\text{oct}} = 1/u + 2/u_{38}, \quad g_{\text{tet}} = 3/u_{18}, \quad g_{\text{oct}}^\phi = 2/u_{18} + 1/u_{12},$$

$$g_{\text{tet1}}^\phi = 3/u_{38}, \quad g_{\text{tet2}}^\phi = 1/u_{18} + 1/u_{38}. \quad (4)$$

These expressions are algebraic examples of the assumed polyhedral-bulk compressibility relations holding for structures with polyhedral linkages.¹⁹

It is also immediate to recover the crystal compressibility as a weighted sum of polyhedral contributions:¹⁷

$$\kappa = \sum_p f_p \kappa_p, \quad f_p = \frac{n_p V_p}{V}. \quad (5)$$

Equations (1)–(5) collect all necessary elements for the polyhedral analysis of the spinel structure.

B. Total energy and EOS fittings

Calculations have been carried out with the CRYSTAL98 package,¹⁶ using the all-electron basis sets reported by Catti *et al.*¹⁰ and the B3LYP approximation.^{20,21} Convergence in total energy E was better than 10^{-5} a.u. in all cases. The B3LYP approximation was extensively used in molecular quantum chemistry and in solid state calculations where it gave accurate descriptions of crystal structures, cohesive energies, and band gaps.^{22,23} We have computed the electronic band structure at selected points of the Brillouin zone for the cubic and orthorhombic structures.²⁴ It is to be noted that our choice of a common basis set for the three polymorphs of MgAl_2O_4 differs from the criterion of separate optimization of the outer shells of the Mg, Al, and O atomic orbitals for the S and T phases used by Catti.¹⁴

To compute the pressure effect, we first find the values of the geometrical parameters that minimize E at a number of fixed volumes using the Melder-Mead algorithm.²⁵ Thus, in the cubic structure, we optimize u for each volume. In the F and T structures, however, we optimize two unit-cell parameters for each volume and keep the internal coordinates fixed to the observed values in CaFe_2O_4 and CaTi_2O_4 , respectively.^{26,27} In this way, a direct comparison with the experimental equilibrium structural parameters can be performed since the diffraction patterns were obtained assuming the same atomic coordinates.⁴ These coordinates can certainly differ from the actual values, but they seem to be very insensitive to the applied pressure.¹⁴

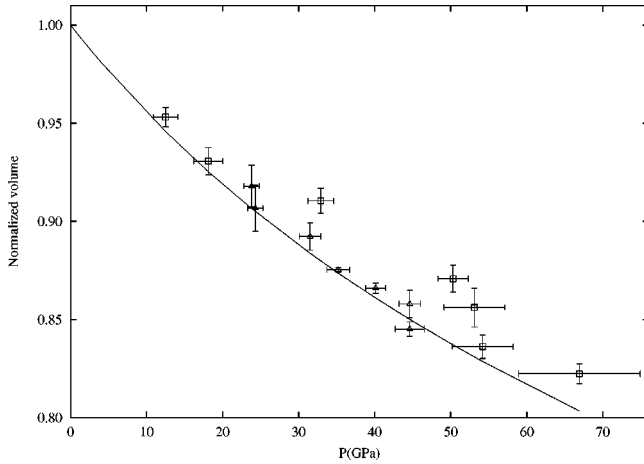


FIG. 2. Normalized volume-applied pressure diagram for the cubic spinel phase of MgAl₂O₄. Points and error bars are taken from Kruger *et al.* (Ref. 8). The solid line is the calculation of this work.

We represent the optimized (E, V) pairs by numerical and analytical empirical functions, including the Vinet's universal EOS,²⁸ as implemented in our GIBBS code.²⁹ The Vinet equation gives the required $p(V)$ relation, the zero-pressure bulk modulus B_0 , and its first-pressure derivative B'_0 . This procedure has been particularly useful in the calculation of second derivatives from (E, V) data.

For any given pressure, a volume can be assigned to each elementary polyhedra by the same fitting procedure. Thus this algorithm gives the EOS parameters of the polyhedra and their compressibilities. Our analyses rest upon the static approximation, i.e., they are performed in the athermal limit with all zero-point energy contributions neglected.

III. RESULTS AND DISCUSSION

A. Polyhedral analysis of the spinel EOS

The static equilibrium configuration for the spinel is found at $a = 8.137 \text{ \AA}$ and $u = 0.2635$, in good agreement with the experimental values: $a = 8.060 \text{ \AA}$ and $u = 0.2624$.³⁰ As the pressure increases, the computed a and u decrease. This direct calculation of the pressure response of the normalized volume can be compared with recent experiments⁸ that found this structure (meta)stable up to 65 GPa. The $V/V_0 - p$ diagram in Fig. 2 shows a good experiment-theory agreement. The best EOS parameters that describe the available experimental data of the S phase are:⁸ $B_0 = 196 \pm 1 \text{ GPa}$, $B'_0 = 4.7 \pm 0.3$, and $B_0 \cdot B''_0 \approx -6$. Our computed values are 201.4 GPa, 3.9, and -5.2. Our value for B''_0 supports the use of hydrostatic-compression data rather than ultrasonic data, that give $B_0 \cdot B'_0 \approx -79 \pm 66$.⁸

In Table I we present the spinel response to hydrostatic pressure in terms of the polyhedral decomposition introduced in Sec. II A. First, we notice that each type of elementary polyhedron shows a different pressure response (see also Fig. 3). From Eq. (3) we see that if u does not change with pressure, the polyhedral and bulk compressibilities coincide. This situation can only be found in fully constrained structures

TABLE I. Decomposition of the bulk compressibility into polyhedral contributions according to our zero-pressure calculations. n_p and f_p are the number and fractional occupation of the polyhedra in the unit cell. f_p^{ideal} refers to the fractional occupation in the $u = 1/4$ structure. The g_p functions are defined in Eqs. (3) and (4). Volumes in \AA^3 and κ_p in GPa^{-1} .

	V_0 (\AA^3)	n_p	f_p	f_p^{ideal}	$\kappa_p \times 10^{-3}$	g_p
unit cell	538.36		1	1	4.965	
AlO ₆	9.402	16	0.2794	$\frac{1}{3}$	4.082	-14.148
MgO ₄	3.816	8	0.0567	$\frac{1}{24}$	5.937	21.6555
O ₆	13.029	16	0.3872	$\frac{1}{3}$	5.343	10.2081
(O ₄) ₁	1.989	8	0.0296	$\frac{1}{24}$	3.423	-26.914
(O ₄) ₂	2.771	48	0.2471	$\frac{1}{4}$	4.723	-1.7528

with rigid polyhedral linkages. Since spinel presents three-dimensional edge-linked structures, the variation of u with pressure is expected to be moderate. Our computed value for $(\partial u / \partial p)$ is $-4.38 \times 10^{-5} \text{ GPa}^{-1}$. This number and the computed zero-pressure g_p functions collected in Table I produce polyhedral compressibilities in the range 4.00×10^{-3} to $6.00 \times 10^{-3} \text{ GPa}^{-1}$, the bulk value being $4.97 \times 10^{-3} \text{ GPa}^{-1}$.

From this table and Fig. 3 we see that the polyhedral volumes reduce upon compression in the order $(\text{O}_4)_1 < \text{AlO}_6 < (\text{O}_4)_2 < \text{bulk} < \text{O}_6 < \text{MgO}_4$, the same trend can be inferred from the experimental data.³¹ This is a general result for normal spinels containing divalent and trivalent cations and having $(\partial u / \partial p) < 0$. Thus empty O₄ tetrahedra have a lower compressibility than MgO₄, whereas AlO₆ is more difficult to compress than the empty O₆ (see also κ_p values in Table I). This behavior can be described recalling the concept of ideal ($u = 1/4$) structure, which defines a reference volume for each elementary polyhedron, and the empirical $B \sim V^{-1}$ relationship,¹⁹ that we assume to hold for empty

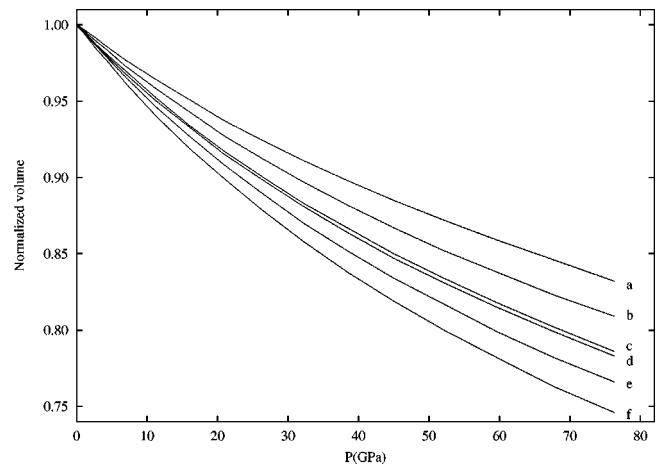


FIG. 3. Pressure response of the normalized polyhedral volumes of the cubic spinel phase of MgAl₂O₄: (a) (O₄)₁, (b) AlO₆, (c) (O₄)₂, (d) bulk, (e) O₆, and (f) MgO₄, according to the present calculation. The response of the bulk volume is included for reference.

TABLE II. Zero-pressure structural data for the ferrite-type and the titanite-type structures of MgAl_2O_4 according to different experimental works and our calculations. Cell parameters in \AA , molecular volume in \AA^3 , B_0 in GPa, and B'_0 in GPa^{-1} .

	Calculated		Experimental			
	this work		Ref. 1	Ref. 3	Ref. 4	
	ferrite	titanite	ferrite	ferrite	ferrite	titanite
a	8.671	2.812	8.631	8.634	8.649	2.778
b	10.08	9.200	9.969	9.966	9.977	9.211
c	2.837	9.588	2.789	2.789	2.785	9.394
V_0	61.87	62.02	60.00	60.00	60.08	60.08
B_0	214.9	214.8		241 ± 3	211 ± 6	206 ± 3
B'_0	4.2	4.9		4 (fixed)	4 (fixed)	4 (fixed)
B''_0	-0.028	-0.037				

polyhedra. From these two ideas we deduce the following estimation for the polyhedral compressibility,

$$\kappa_p^{\text{est}} = \kappa \frac{f_p}{f_p^{\text{ideal}}}, \quad (6)$$

which works with an average error smaller than 5%.

The results of our calculations indicate that elementary polyhedra having volumes larger (smaller) than the corresponding ideal volume show compressibilities larger (smaller) than the bulk value. The observed relationship between $\kappa_p - \kappa$ and $V_p - V$ means that the response of the S phase to the applied pressure can be understood as an ionic rearrangement toward the ideal close-packed structure. Thus we can say that the external pressure induces a transformation that increases the local symmetry of the crystal by reducing the distortion of the oxide sublattice.

B. Structure and EOS of the orthorhombic polymorphs

The structure of the two orthorhombic phases can be described in terms of cationic polyhedra: Al^{3+} shows a pseudo-octahedral coordination with four different Al-O distances, all of them similar to those in the cubic structure. Mg^{2+} is surrounded by eight oxides, six at the corners of a trigonal prism and close the other two to the centers of two prism faces.²⁶ These polyhedra have five (three) different Mg-O distances in the F (T) phase. The two basic differences between these structures seem to be the existence of two non-equivalent Al^{3+} ions in the F form and the smaller polyhedral distortion in the T form.

The experimental studies on these two phases^{1,3,4} use the atomic coordinates of CaFe_2O_4 and CaTi_2O_4 to describe the zero-pressure unit cell. Both forms are nearly 10% denser than the cubic spinel. They are considered to be the most dense known structures with AB_2O_4 stoichiometry.^{1,2} There is a remarkable agreement among the three experimental values of the zero-pressure molecular volume V_0 for the quenched F form, namely, 60.00, 60.00, and 60.08 \AA^3 . The zero-pressure structure of the T phase has only been experimentally described by Funamori *et al.*,⁴ who gave $V_0 = 60.08 \text{ \AA}^3$.

In Table II we present our results for the pressure response of the unit lengths (a, b, c) of the orthorhombic phases. First, we notice that the calculated zero-pressure densities are also higher than the density of the spinel. The predicted increment agrees with the experimental result. We also find that the two phases have very similar V_0 values, titanite's being 0.2% higher. Our calculation does not permit a definite prediction of the relative densities of these two phases since their close molecular volumes may demand an accurate determination of the internal coordinates. In this respect, our results overestimate the equilibrium volume of the T phase by about 2% in comparison with the fully optimized B3LYP unit cell calculated by Catti,¹⁴ but a similar result may be expected for the F phase. In Table II we can observe that the theoretical and experimental values of the unit cell parameters (a, b, c) agree within a 2%.

Let us now turn to the EOS results. B_0 values for the orthorhombic polymorphs have been reported from Birch fittings³² to the observed p - V data. In the range $0 \leq p \leq 8.8$ GPa, Yutani *et al.*³ found $B_0 = 241 \pm 3$ GPa for the F phase, taking $B'_0 = 4$. They also found that changing B'_0 from 2 to 6 moves B_0 from 233 to 252 GPa. A lower value ($B_0 = 211 \pm 6$, $B'_0 = 4$ fixed) for this structure is proposed by Funamori *et al.*⁴ using only the volume value at 33.4 GPa. For the T phase, they obtained $B_0 = 206 \pm 3$, $B'_0 = 4$ fixed. It is noteworthy, however, that a *single* Birch-Murnaghan curve with $B_0 = 210$ GPa and $B'_0 = 4$ describes correctly all the observed data for the two polymorphs,⁴ including those of Yutani *et al.*³ Since V_0 is almost the same for the two phases, the relative value of B_0 is the key quantity to confirm a pressure-induced $F \rightarrow T$ transition.

Our EOS analysis covers the $0 \leq p \leq 48$ GPa range for the F phase and the $0 \leq p \leq 65$ GPa range for the T phase. We have found that these structures have a nearly isotropic pressure response: the three unit lengths decrease at similar rates with increasing pressure in both phases. Linear compressibilities computed with a monodimensional Vinet-like equation^{17,33} are roughly $\kappa_a = 1.7 \times 10^{-3} \text{ GPa}^{-1}$, $\kappa_b = 1.7 \times 10^{-3} \text{ GPa}^{-1}$, and $\kappa_c = 1.3 \times 10^{-3} \text{ GPa}^{-1}$ for the two phases. From these numbers we recover B_0 values consistent with those deduced from p - V data (see Table II). Although no experimental linear compressibilities are available, the measured (a, b, c) lengths reveal a nearly isotropic behavior in the two polymorphs, the T form showing a lower splitting of the compressibilities. Our calculation gives almost identical bulk moduli, $B_0 \sim 215$ GPa, for the two phases in agreement with Funamori *et al.*⁴ At 33.4 GPa, we obtain $V/V_0 = 0.8842$ for the F structure (0.8838 observed) and 0.8200 for the T form, where there is a single observed p - V point, at 64.3 GPa, with $V/V_0 = 0.8135$. We see that our calculation gives a rather satisfactory description of the equilibrium structures and pressure response of these two orthorhombic phases.

C. Spinel decomposition and cubic-to-orthorhombic transitions

In this section we study the stability of the cubic form against compression in the static approximation. The exis-

tence of kinetic hindrances associated with the decomposition of MgAl_2O_4 into the oxide mixture $\text{MgO} + \alpha\text{-Al}_2\text{O}_3$ and subsequent transformations into orthorhombic phases is well established. The oxides and the high-pressure polymorphs have always been observed on heated samples,⁴ but Kruger *et al.*⁸ found that the *S* form is (meta)stable up to 65 GPa at room temperature. In the experiments of Funamori *et al.*,⁴ laser-heated samples with temperature peaks between 2000 and 3000 K decomposed first into the oxide mixture, the *F* phase is then identified around 30 GPa, and finally the *T* phase is proposed as the most stable form above ~ 40 GPa. In all runs, residual cubic spinel was observed, “but its amount decreased significantly with pressure.”⁴ Irifune *et al.*¹ found an oxide mixture at 15 GPa after heating either at 1000 or 1500 °C, and then “the sample was found to convert mostly” to the *F* structure at 26 GPa and 1500 °C. This orthorhombic phase was thus obtained from the oxide mixture. It may be well to recall here that a direct transformation from the *S* form to the *F* or *T* form without previous oxide decomposition has recently been reported for MgCr_2O_4 .³⁴

The present calculation can not describe the kinetics of the transformations but it can be used to assign the high-pressure polymorphs to the regions of lower enthalpy in the phases diagram, since H is the appropriate thermodynamic potential in the static approximation. We expect that inclusion of thermal effects would slightly modify the main features of the stability relations discussed here. To describe the static decomposition of MgAl_2O_4 into its simple oxides, we performed calculations on MgO and $\alpha\text{-Al}_2\text{O}_3$ using the computational parameters adopted for the three polymorphs. Our structure and EOS calculations are in good agreement with those of Catti *et al.*¹⁰ and with the experimental data collected in that reference. From our computed zero-pressure molecular volumes and bulk moduli [$V_0 = 18.87 \text{ \AA}^3$ (MgO), $V_0 = 43.42 \text{ \AA}^3$ ($\alpha\text{-Al}_2\text{O}_3$), $B_0 = 170.3 \text{ GPa}$ (MgO), and $B_0 = 249.5 \text{ GPa}$ ($\alpha\text{-Al}_2\text{O}_3$)], we obtain $V_0 = 62.29 \text{ \AA}^3$ and $B_0 = 218.6 \text{ GPa}$ for the oxide mixture, two numbers very close to those found for the orthorhombic polymorphs.

At zero pressure, the cubic phase is calculated to be 43.9, 103.7, and 157.6 kJ/mol more stable than the oxide mixture, the *F* phase, and the *T* phase, respectively. As the pressure increases, these differences reduce and we find that the thermodynamically stable phase changes. According to our calculations, there is not a $S \rightarrow \text{oxide mixture} \rightarrow F \rightarrow T$ sequence, since the mixture has smaller enthalpy than the two orthorhombic structures for all pressures. The *F* polymorph has also lower enthalpy than the *T* form. Nevertheless, we predict transformations from the *S* to the oxide mixture at ~ 15 GPa, to the *F* form at ~ 35 GPa, and to the *T* form at ~ 62 GPa. These results can be seen in the stability diagram of Fig. 4.

The resulting $V/V_0 - p$ diagram is depicted in Fig. 5. In this plot, V_0 refers to the zero-pressure molecular volume of the *S* structure. We indicate with arrows the change of volume involved in the transitions. At the transition pressure p_t , the relative change $\Delta V_t = [V_2(p_t) - V_1(p_t)]/V_1(p_t)$, where 2 and 1 stand, respectively, for the final and *S* phases, is about -7% for the three transitions. This result differs slightly from

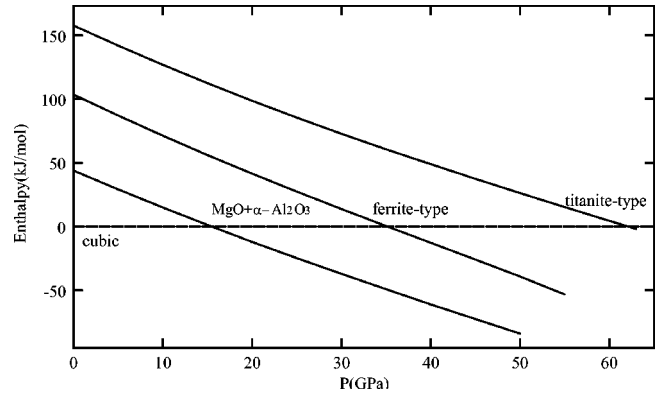


FIG. 4. Thermodynamic stability diagram of MgAl_2O_4 in the static approximation. The equilibrium curves are the enthalpy differences $H(p;J) - H(p;S)$, where S stands for the cubic spinel phase and J runs over the mixed-oxide phase, the ferrite-type phase, and the titanite-type phase, as indicated.

the relative change of V_0 since the compressibility of the cubic spinel is only slightly greater than those of the high-pressure phases. We note that the small differences among the computed $V/V_0 - p$ curves of the three phases cast doubts about the viability of a $F \rightarrow T$ transition. According to our calculations, the thermodynamic requirement of volume reduction for pressure-induced phase transitions is not accomplished in this case. For the oxide mixture $\rightarrow F$ transition the volume reduction at the observed $p_t = 25\text{--}30$ GPa is almost negligible.

We have also evaluated the changes in compressibility and electronic band structure across the cubic-to-orthorhombic phase transitions. We found ΔB_t values of +5% and +7% at the corresponding predicted p_t for the $S \rightarrow F$ and the $S \rightarrow T$ transitions, respectively. The calculated ΔB_0 turns out to lie within these two figures. At a given pressure, the computed B for the orthorhombic structures are nearly identical. Thus $\text{sgn}(\Delta B) = \text{sgn}(\Delta B_0)$, and the denser structures are predicted to be the less compressible.

The computed electronic band structure reveals that the *S*, *F*, and *T* phases are insulators at $p = 0$, with direct band gaps of 7.90, 7.07, and 6.53 eV, respectively, that increase with

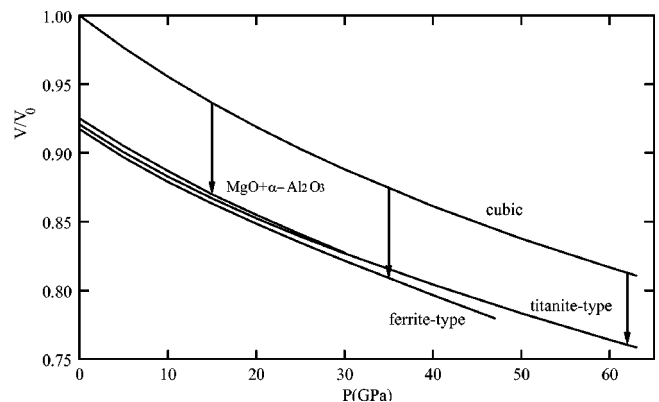


FIG. 5. Calculated normalized volume-pressure diagram of all phase of MgAl_2O_4 studied in this work. V_0 is the zero-pressure molecular volume of the cubic spinel structure.

pressure at a rate of ~ 0.047 eV/GPa for the cubic and the two orthorhombic phases. The bandgap is reduced by some 0.5 eV at $p=p_t(S \rightarrow F)$ and by nearly 1.0 eV at $p=p_t(S \rightarrow T)$. On the other hand, the valence bandwidth increases with pressure at about 0.025 eV/GPa in the three polymorphs. We calculate the broadening of this band at the transition pressure to be 1.3 eV ($S \rightarrow F$) and 2.1 eV ($S \rightarrow T$).

Changes in observable properties induced by the phase transitions can be related to different atomic arrangements in the crystals. The Al^{3+} coordination is sixfold in all cases but that of Mg^{2+} is fourfold in the cubic spinel, sixfold in MgO , and eightfold in the orthorhombic structures. Moreover, the volume of the distorted AlO_6 octahedra is almost the same in the four phases: V_{oct} is only $\sim 1.4\%$ lower in the high-pressure phases, at $p=0$. Thus the higher density of the orthorhombic structures can be traced back to the unit-cell volumen reduction due to a more effective packing of the anions surrounding the Mg^{2+} ions. In fact, $\Delta V_{\text{oct}}(p_t)$ is much lower than the bulk transition volume.

In this way, the atomic displacements across the $S \rightarrow F$ and $S \rightarrow T$ transitions are clearly related to the environment evolution of the divalent cation. For example, at $p_t(S \rightarrow F) = 35$ GPa, the cubic phase has four Mg-O distances of 1.848 Å, and six Al-O distances of 1.854 Å. At the same pressure, the average of the eight Mg-O and the six Al-O shortest distances in the F phase are 2.200 and 1.837 Å, respectively. A similar behavior is found for the $S \rightarrow T$ transition. In these pressure-induced transitions, we find that the aluminum coordination does not change and the Al-O bond lengths remain almost unmodified, whereas the magnesium coordination increases and the Mg-O bond lengths become larger, to make the formation of new bonds feasible.

These bonding effects can be further characterized by the changes in bond strength associated with the transition. This property can be estimated by the reduction rate of the bond length upon compression. We compute this effect from the results of our calculations but the same conclusions can be derived using experimental data. Figure 6 collects these reductions. In the S structure, the Mg-O and Al-O distances are about 1.94 Å at $p=0$. The mean Mg-O distances in the other systems are 2.11 Å (MgO), 2.30 Å (F), and 2.33 Å (T). The mean Al-O bondlengths are 1.93 Å ($\alpha\text{-Al}_2\text{O}_3$), 1.92 Å (S), and 1.92 Å (T). These numbers are consistent with the results discussed above which present, in the S phase, aluminum octahedra harder to compress than magnesium tetrahedra. In the oxide mixture, these two bonds shrink with applied pressure as they do in the spinel. The orthorhombic structures display a different picture: the strength of the Al-O bond slightly decreases, that of the Mg-O bond increases and their bond compressibilities become nearly the same.

Thus, the relatively short Mg-O bonds in the cubic phase tetrahedra become larger in the eightfold coordination of the orthorhombic phases but the higher coordination enhances their strength and brings their compressibility close to that shown by the Al-O bonds. This effect suggests that we could tentatively assign the origin of the ‘‘incipient lattice instability’’ of the spinel phase reported by Chopelas and Hofmeister³⁵ to vibrational modes associated with the Mg-O bonds.

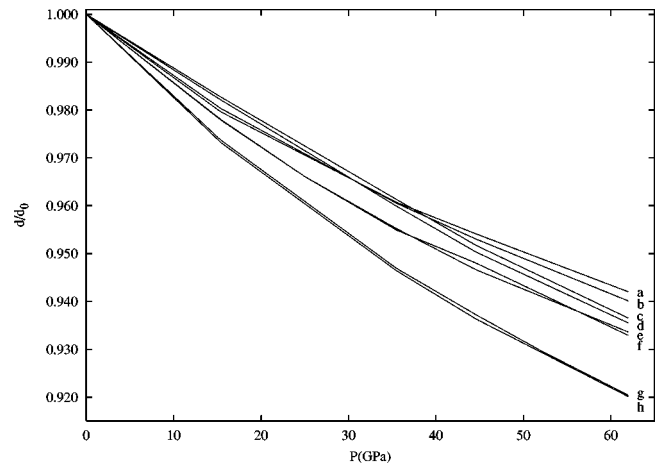


FIG. 6. Calculated normalized distance-pressure diagram for Mg-O and Al-O bonds in the four phases of MgAl_2O_4 studied in this work. Curves *a*, *b*, *c*, and *e* stand for Al-O bond lengths in $\alpha\text{-Al}_2\text{O}_3$, the S , T , and F phases, respectively. Curves *d*, *f*, *g*, and *h* are Mg-O bond lengths in the T , F , MgO , and the S phases. d_0 is the zero-pressure distance for each bond.

IV. CONCLUSIONS

We have performed quantum-mechanical calculations on the cubic spinel phase and two polymorphs of MgAl_2O_4 , as well as on the oxide components of this crystal: MgO and $\alpha\text{-Al}_2\text{O}_3$. From them we analyze the equilibrium structures, equations of state, and pressure-induced phases diagram of this material. We use density-functional-theory methods with the hybrid, nonlocal B3LYP approximation as implemented in the CRYSTAL98 code.¹⁶ We find good general agreement with recent experimental and theoretical data on equilibrium unit-cell parameters and compressibilities, and obtain orthorhombic phases $\sim 10\%$ denser than the cubic spinel, with very similar zero-pressure bulk moduli about 215 GPa. Linear compressibilities reveal an almost isotropic response of these polymorphs to applied hydrostatic pressure.

The polyhedral decomposition of the spinel structure permits to identify the response of the polyhedral volumes to compression. Although some of the empty polyhedra turn out to be harder to compress than the occupied ones, we have rationalized the whole behavior by invoking the ideal ($u = 1/4$) anion packing and the empirical $B \sim V^{-1}$ law. The resulting image depicts the spinel response to compression as an ionic rearrangement towards the ideal packing.

The computed phase stability diagram fails to predict the transition $\text{spinel} \rightarrow \alpha\text{-Al}_2\text{O}_3 + \text{MgO} \rightarrow \text{ferrite-type} \rightarrow \text{titanite-type}$ phase sequence, but the calculation tells that all the high-pressure phases can be obtained from the cubic spinel upon compression. From this diagram we obtain transition pressures using the static ($T=0$ and zero-point effects neglected) approximation, and from these quantities we compute transition values for a series of thermodynamic and electronic properties, including volume, compressibility, band gap, and valence bandwidth. We also found that the pressure-induced ferrite-to-titanite transition is incompatible to our structural simulation because we obtain a positive transition volume in this direction. These result should be

taken with caution due to our incomplete optimization of the unit-cell coordinates in the orthorhombic structures.

The analysis of the cationic environments in different circumstances reveals that the increasing coordination of the Mg²⁺ in passing from the spinel to the high-density phases controls the microscopic changes associated to these transformations. Whereas the AlO₆ octahedra maintain the coordination, length, and compressibility across the phase transition, the Mg-O bonds become larger and less compressible. In the spinel structure these two types of bond show comparable lengths but different compressibilities. In the orthorhombic polymorphs the bond lengths become different but the compressibilities are about the same. In view of this peculiar behavior, we finally advance the conjecture that the

comparative weakness of the Mg-O bonds in the spinel might be at the origin of the lattice instability of this structure.

ACKNOWLEDGMENTS

Financial support from the Spanish MCYT (Projects Nos. BQU2000-0466 and BQU2000-1425-C03-C02) and Fundació Bancaixa (Project No. P1A99-02) are gratefully acknowledged. J.M.R. and L.G. thank the Spanish MECED for visiting professor at UJI and doctoral grants, respectively. Computer facilities of the Servei d'Informàtica (UJI) are further acknowledged.

-
- ¹T. Irifune, K. Fujino, and E. Ohtani, *Nature (London)* **349**, 409 (1991).
- ²A. F. Reid and A. E. Ringwood, *Earth Planet. Sci. Lett.* **6**, 205 (1969).
- ³M. Yutani, T. Yagi, H. Yusa, and T. Irifune, *Phys. Chem. Miner.* **24**, 340 (1997).
- ⁴N. Funamori, R. Jeanloz, J. H. Nguyen, A. Kavner, W. A. Caldwell, K. Fujino, N. Miyajima, T. Shinmei, and N. Tomioka, *J. Geophys. Res.* **103**, 20 813 (1998).
- ⁵L.-G. Liu, *Geophys. Res. Lett.* **2**, 9 (1975).
- ⁶L.-G. Liu, *Earth Planet. Sci. Lett.* **41**, 398 (1978).
- ⁷H. Schafer, W. F. Muller, and U. Hornemann, *Phys. Chem. Miner.* **9**, 248 (1983).
- ⁸M. B. Kruger, J. H. Nguyen, W. Caldwell, and R. Jeanloz, *Phys. Rev. B* **56**, 1 (1997).
- ⁹P. D'Arco, B. Silvi, C. Roetti, and R. Orlando, *J. Geophys. Res.* **96**, 6107 (1991).
- ¹⁰M. Catti, G. Valerio, R. Dovesi, and M. Causà, *Phys. Rev. B* **49**, 14 179 (1994).
- ¹¹S.-D. Mo and W. Y. Ching, *Phys. Rev. B* **54**, 16 555 (1996).
- ¹²A. Martín Pendás, A. Costales, M. A. Blanco, J. M. Recio, and V. Luaña, *Phys. Rev. B* **62**, 13 970 (2000).
- ¹³J. M. Recio, R. Franco, A. Martín Pendás, M. A. Blanco, L. Pueyo, and R. Pandey, *Phys. Rev. B* **63**, 184101 (2001).
- ¹⁴M. Catti, *Phys. Chem. Miner.* **28**, 729 (2001).
- ¹⁵A. Beltrán, L. Gracia, J. Andrés, R. Franco, and J. M. Recio, *High Press. Res.* **22**, 447 (2002).
- ¹⁶V. R. Saunders, R. Dovesi, C. Roetti, M. Causà, N. M. Harrison, R. Orlando, and C. M. Zicovich-Wilson, *CRYSTAL98 User's Manual* (University of Torino, Torino, 1998).
- ¹⁷M. Calatayud, P. Mori-Sánchez, A. Beltrán, A. Martín Pendás, E. Francisco, J. Andrés, and J. M. Recio, *Phys. Rev. B* **64**, 184113 (2001).
- ¹⁸T. Yamanaka and Y. Takeuchi, *Z. Kristallogr.* **165**, 65 (1983).
- ¹⁹R. M. Hazen and L. W. Finger, *J. Geophys. Res.* **84**, 6723 (1979).
- ²⁰A. D. Becke, *J. Chem. Phys.* **98**, 5648 (1993).
- ²¹C. Lee, W. Yang, and R. G. Parr, *Phys. Rev. B* **37**, 785 (1988).
- ²²C.-H. Hu and D. P. Chong, in *Encyclopedia of Computational Chemistry*, edited by P. von Ragué Schleyer (Wiley, Chichester, 1998).
- ²³J. Muscat, A. Wander, and N. M. Harrison, *Chem. Phys. Lett.* **342**, 397-401 (2001).
- ²⁴C. J. Bradley and A. P. Crácknell, *The Mathematical Theory of Symmetry in Solids* (Clarendon Press, Oxford, 1972).
- ²⁵J. A. Melder and R. Mead, *Comput. J. (UK)* **7**, 308 (1965).
- ²⁶B. F. Decker and J. S. Kasper, *Acta Crystallogr.* **10**, 332 (1957).
- ²⁷B. G. Hyde and S. Andersson, *Inorganic Crystal Structures* (Wiley, New York, 1988).
- ²⁸P. Vinet, J. H. Rose, J. Ferrante, and J. R. Smith, *J. Phys.: Condens. Matter* **1**, 1941 (1989).
- ²⁹M. A. Blanco, E. Francisco, and J. M. Recio, the GIBBS code, 1997.
- ³⁰P. Fischer, *Z. Kristallogr.* **124**, 275 (1967).
- ³¹L. W. Finger, R. M. Hazen, and A. M. Hofmeister, *Phys. Chem. Miner.* **13**, 215 (1986).
- ³²F. Birch, *J. Geophys. Res.* **57**, 227 (1952).
- ³³E. Francisco, M. A. Blanco, and G. Sanjurjo, *Phys. Rev. B* **63**, 094107 (2001).
- ³⁴Z. Wang, H. S. C. O'Neill, and P. Lazor, and S. K. Saxena, *J. Phys. Chem. Solids* **63**, 2057 (2002).
- ³⁵A. Chopelas and A. M. Hofmeister, *Phys. Chem. Miner.* **18**, 279 (1991).